JAXA Research and Development Report

Momentum Balance Model of Flow Field with Pseudo-Shock

Takeshi KANDA , Kouichiro TANI

March 2007

Japan Aerospace Exploration Agency

JAXA Research and Development Report

宇宙航空研究開発機構研究開発報告

Momentum Balance Model of Flow Field with Pseudo-Shock

擬似衝撃波を含む流れの運動量釣合モデル

Takeshi KANDA , Kouichiro TANI

苅田　丈士、谷　香一郎

Combined Propulsion Research Group, Institute of Aerospace Technology

総合技術研究本部　複合推進研究グループ

Japan Aerospace Exploration Agency

宇宙航空研究開発機構

Momentum Balance Model of Flow Field with Pseudo-Shock*

Takeshi KANDA[*1] and Kouichiro TANI[*1]

擬似衝撃波を含む流れの運動量釣合モデル*

苅田丈士[*1]、谷 香一郎[*1]

ABSTRACT

The length of a pseudo-shock was estimated with a new momentum balance model. In this simple model, it is presumed that there is no wall friction in the region of the pseudo-shock. Inflow conditions are specified at a boundary sufficiently upstream of the pseudo-shock. The outflow boundary condition is applied with, for example, specified pressure or choking. The outflow impulse function is balanced with the inflow impulse function, the wall friction upstream of the pseudo-shock, and the reaction force from the wall. The starting position of the pseudo-shock is determined through balance of the forces in this model, and the length of the pseudo-shock is also determined. The model was applied to several kinds of flow fields, for example, straight ducts with and without a backward-facing step, and divergent ducts. The model was also applied to the diffuser of an ejector-jet, in which two gases flowed in parallel. The calculated results reasonably agreed with the experimental results within the scope of preliminary application. The starting position of the pseudo-shock was primarily dominated by the reaction force in the divergent duct. Several features of the pseudo-shock were discussed with the present model.

概　　要

　新しく提案する運動量釣合モデルを用いて、擬似衝撃波長さの推算を行った。この簡単なモデルでは、擬似衝撃波領域の壁面摩擦を 0 と仮定する。流入境界条件は擬似衝撃波の十分に上流で規定され、下流境界条件は出口圧力あるいはチョーク（閉塞）条件などで与えられる。流出インパルスファンクションは、流入インパルスファンクション、摩擦力、壁面からの反力と釣合う。この運動量釣合いモデルでは擬似衝撃波の開始位置、すなわち擬似衝撃波の長さは、この力のバランスが取れるように決められる。このモデルをステップのある／ない平行ダクトや、拡大管内の流れに適用してみた。2 流が平行に流れるエジェクタージェットのディフューザー部にも適用してみた。このモデルは初期段階での検討用のモデルである。この点に鑑みると、計算結果は実験結果によく一致した。拡大管内の流れでは、擬似衝撃波開始位置は主に壁面反力に依存した。このモデルを用いて、擬似衝撃波の幾つかの特徴についても議論を行った。

Nomenclature

A = cross section, papameter of Eqs. (7) and (17)
a = papameter of Eq. (7)
B = parameter of Eqs. (7) and (17)
b = parameter of Eq. (7)
Cp = specific heat at constant pressure
D = diameter of duct, hydraulic diameter
F = impulse function, force
f = streamwise component of force
H = Duct height
h = enthalpy
L = duct length
M = Mach number
$\dot{m}$ = mass flow rate
P = pressure
q = heat release

R = gas constant
Re = Reynolds number
S = papameter of Eq. (16)
T = temperature
u = velocity
w = Crocco number, $u/\sqrt{2Cp \cdot T_t}$
x = streamwise distance
γ = ratio of specific heats
μ = viscosity
θ = boundary layer momentum thickness

Superscript

$*$ = sonic state

Subscripts

aw = adiabatic wall
b = bleeding
d = duct
div = divergent duct part

e	= outflow	
f	= friction	
i	= inflow	
p	= pseudo-shock, state at the exit of	
	pseudo-shock	
r	= reaction	
$step$	= step	
t	= total	
th	= throat	
w	= wall	
1	= upstream of pseudo-shock, entrance,	
	primary flow	
$1b$	= after bleeding and upstream of pseudo-	
	shock	
2	= downstream of pseudo-shock,	
	secondary flow	

Fig. 1 Schematic of flow field with pseudo-shock.

I. Introduction

The pseudo-shock which generally appears in the deceleration process from supersonic to subsonic flow in a duct has been studied.[1,2] Figure 1 shows a schematic diagram of a flow field with a pseudo shock. Supersonic flow enters a duct. Some boundary condition is applied at the exit, for example, a static pressure condition or a choking condition. When the pressure at the exit of the duct is high, a pseudo-shock is produced in the duct. Such a flow field appears in supersonic devices, that is, diffusers of the supersonic wind tunnel, diffusers of the ramjet engine and the ejector-jet engine, and isolator/combustors of the scramjet engine and the dual-mode engine. In the diffusers of the wind tunnel, the static pressure condition is usually applied at the exit. In the engines, the choking condition is applied.

The shock waves interact with the inflow boundary layer, and the layer separates from the wall surface or becomes thicker. Herein, the region of the pseudo-shock is from the beginning of the interaction to the position at the maximum pressure, that is, the region where the separation can exist. Downstream of the maximum pressure point, the separated flow will be attached again. In the region of the pseudo-shock, flow was separated from the wall, and there was little or negative friction force on the wall surface.[3-6] In some papers,[4,5] separation was not reported, but quick thickening of the boundary layer in the region of the pseudo-shock was reported. In such case, friction in
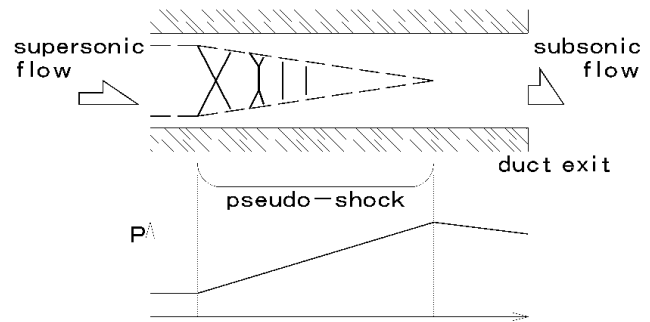
the pseudo-shock would be decreased, even though there is no separation. The friction force comes into play in the attached flow upstream and downstream of the pseudo-shock. The flow field is complicated, including supersonic flow, subsonic flow and transonic flow.

There are several analytical models of the pseudo-shock.[2,7-9] Crocco proposed a shockless model.[2] In his model, the dissipative region spreads toward the isentropic region. He tried to estimate local pressure in the pseudo-shock by a ratio of the dissipation region. The model did not show the location of the local pressure or the length of the pseudo-shock. As for the length of the pseudo-shock, many researchers tried to present a way of estimation of the length. Ikui and others have presented modifications[7,8] to the Crocco model and have estimated length of the pseudo-shock. Zimont and Ostras have also presented a modification[9] of the Crocco model. In these modified models, the region investigated is limited to that within the pseudo-shock. The length of the pseudo-shock was attained from analysis of the flow structure in the pseudo-shock in these models. Empirical universal equations have been presented for a straight cylindrical duct[10] and a rectangular straight duct.[11] These equations show good agreement with experimental results. In the divergent duct, no universal empirical equation has been attained. Only specific equations for some test results were attained.[12]

In a flow field with a pseudo-shock, the downstream boundary condition is specified with, for example, pressure or choking at the exit of the duct. When pressure is specified at the exit, Mach number is uniquely determined as follows under conservation of mass flow rate and energy.

$$\dot{m} = \rho \cdot u \cdot A$$
$$= PA \sqrt{\frac{\gamma}{RT_t}} \cdot M \sqrt{1 + \frac{\gamma - 1}{2} M^2} \qquad (1)$$

Then, impulse function is also determined at the exit.

$$F = \dot{m}u + PA$$
$$= \dot{m} \frac{\sqrt{\gamma \cdot R \cdot T_t}}{\sqrt{1 + \frac{\gamma - 1}{2} M^2}} \left(M + \frac{1}{\gamma \cdot M} \right) \qquad (2)$$

When choking condition is applied to the downstream boundary, the impulse function is determined, as can be seen at $M = 1$ in Eq. (2).

Supersonic flow enters from the upstream boundary. When the mass flow rate and the total energy are conserved, the impulse function at the exit is different from that at the entrance of the duct. The force should be balanced with the friction force on the wall and the reaction force in the divergent duct irrespective of the flow structure inside the pseudo-shock. In the straight duct, the force balance is achieved by only the friction force.

In the present paper, a new one-dimensional, analytical model is presented for the estimation of the length of the pseudo-shock. In this model, the upstream boundary is set sufficiently upstream of the pseudo-shock. For the force balance, the upstream and the downstream regions of the pseudo-shock are included in discussion. In the previous analytical models, only the inside flow structure of the pseudo-shock was studied, but these regions are not included in specifying process of the length of the pseudo-shock. In the present model, friction on the wall in the pseudo-shock is presumed to be nil. The length of the pseudo-shock is estimated by inflow and outflow momentum balance. The length of the pseudo-shock is studied from the outside of the pseudo-shock here. This model can be applied to a divergent or convergent duct, as well as a straight duct.

The characteristics of the pseudo-shock are also discussed, based on the present modeling of the flow field. Backward-facing step is adopted for suppression of upstream extension of the pseudo-shock in some supersonic devices, for example, the scramjet engine. Its effectiveness is examined from the viewpoint of momentum balance. For the scramjet engine, required

length of the isolator between the inlet and the combustor is also examined. Effects of height of the boundary layer, pressure at the exit of the duct, throttling and bleeding on the starting position of the pseudo-shock are also examined from the viewpoint of the momentum balance.

II. Features of the Model and the Calculation Procedure

Figure 2 shows a schematic of the present one-dimensional model. In this model, the upstream boundary is sufficiently upstream of the pseudo-shock, and the inflow conditions are specified there. Friction on the wall in the pseudo-shock is presumed to be nil; friction is nil in the duct with a length of L_p. It is difficult to specify the end position of the pseudo-shock in the divergent duct.[13] Here, the end position of the pseudo-shock is set at the end of the pressure increase in the duct. In the region with an adverse pressure gradient, separation may exist. Even if the flow is not separated, friction force will be small.

In the present model, the starting position of the pseudo-shock depends on the balance among the inflow impulse function, F_i, the outflow impulse function, F_e, the frictions of the attached flow upstream of the pseudo-shock, f_{f1} and downstream of the shock, f_{f2}, and the reaction forces from the wall upstream of the pseudo-shock, f_{r1} and in the pseudo-shock, f_{rp}.
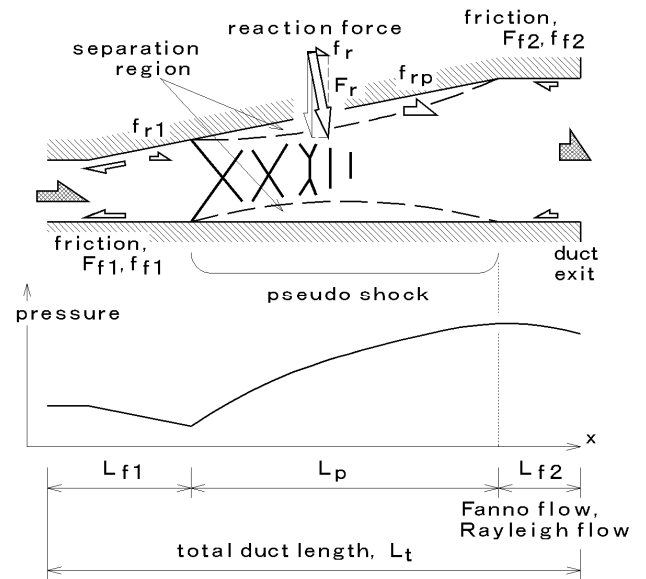

Fig. 2 Schematic of momentum balance model.

$$F_e = F_i + f_{r1} + f_{rp} - f_{f1} - f_{f2} \qquad (3)$$

This relation stands up when friction on the wall in the pseudo-shock is sufficiently small, irrespective of the flow structure in the pseudo-shock. When the downstream boundary is given at the end of the pseudo-shock, that is, when $L_{f2} = 0$, this model can be simplified as below:

$$F_e = F_i + f_{r1} + f_{rp} - f_{f1} \qquad (4)$$

Force balance is attained between the entrance and the exit of the flow field by changing the starting position of the pseudo-shock, namely, the length of the duct upstream of the pseudo-shock, L_{f1}. Both the reaction force, $f_{r1} + f_{rp}$, and the friction force between the upstream boundary and the pseudo-shock, f_{f1}, change due to the starting position of the pseudo-shock. When the duct is straight, the model is further simplified due to lack of reaction force from the wall.

$$F_e = F_i - f_{f1} \qquad (5)$$

The length of the pseudo-shock in the divergent duct or the straight duct, L_p, is calculated with the total length of the duct length, L_t, and length of the attached flow upstream of the pseudo-shock, L_{f1}, as follows.

$$L_P = L_t - L_{f1} \qquad (6)$$

When the downstream straight duct is not omitted, namely, $L_{f2} > 0$, another condition is necessary to specify the length of the pseudo-shock in the flow field.

The previous models for prediction of the length of the pseudo-shock were constructed based on the inside flow structure of the pseudo-shock, whereas the present model does not include modeling of this structure. Pressure distribution in the pseudo-shock would be specified from the flow structure inside the pseudo-shock. However, two pressures, that is, the pressure at the staring position and the pressure at the end of the pseudo-shock, are specified or attained in the present model. Therefore, the pressure in the pseudo-shock is linearly interpolated here. The way in which the pressure distribution is modeled in the pseudo-shock affects f_{rp} and L_p in the divergent duct but does not affect L_p in the straight duct.

This model can be applied to the pseudo-shock with separation. Therefore, inflow supersonic flow should be faster than about Mach 1.5. Below this

Mach number, separation is not produced and the flow field does not contain a pseudo-shock.[2] This model cannot be applied to a shock-train, either, in which flow is supersonic at the exit of the duct and properties are generally not uniform on the exit plane.[1]

Flow condition at the end of the pseudo-shock is calculated with conservation of mass, energy, and impulse function. The condition is different from that behind the normal shock in the inviscid flow because of a decreased impulse function due to the boundary layer upstream of the pseudo-shock. In this model, there is no friction on the wall in the region of the pseudo-shock. For example, when the duct is straight, the impulse function at the starting position of the pseudo-shock is the same as that at the end of the pseudo-shock. Thus, the pressure at the end of the pseudo-shock agrees with the pressure behind the normal shock, including the decrease of the inflow impulse function by the boundary layer.[14]

III. Results and Discussion

In this chapter, first, the lengths of a pseudo-shock calculated with the present model are compared with the measured ones in ducts of simple configuration such as straight ducts and divergent ducts. Next, this model is applied to a dual-mode combustor and a diffuser of an ejector.

A. Pseudo-Shock in a Straight Duct

Specified pressure is frequently applied as a downstream boundary condition in the tests of a pseudo-shock. Length of the pseudo-shock was calculated under specification of pressure at the downstream boundary and compared with the experimentally measured one. The upstream boundary condition was specified at some position apart from the pseudo-shock, for example, the exit of the supersonic facility nozzle. The maximum pressure at the end of the pseudo-shock was specified as the downstream boundary condition. When pressure at the exit of the duct was largest, the pressure was the downstream boundary condition. The length of the pseudo-shock was from the position where pressure began to increase from pressure of the free stream to the position at the largest pressure (Fig. 2). Friction upstream of the pseudo-shock was calculated with a formula of van Driest.[15]

$$\frac{\sin^{-1} A + \sin^{-1} B}{\sqrt{C_f \left(T_{aw}/T_e - 1 \right)}} \approx 4.15 \log_{10} \left(Re_x C_f \frac{\mu_e}{\mu_w} \right) + 1.7 \tag{7}$$

Here,

$$A = \frac{2a^2 - b}{\sqrt{b^2 + 4a^2}} \tag{8}$$

$$B = \frac{b}{\sqrt{b^2 + 4a^2}} \tag{9}$$

$$a = \sqrt{\frac{\gamma - 1}{2} M_e^2 \frac{T_e}{T_w}} \tag{10}$$

$$b = \left(\frac{T_{aw}}{T_w} - 1 \right) \tag{11}$$

Figure 3 shows a comparison of the lengths of the pseudo-shock calculated with the present model with the experimental ones. The lengths of the pseudo-shock are normalized with a hydraulic diameter. Its definition is approximately expressed as below:

$$D \approx 4 \times \text{(cross sectional area) / (wetted perimeter)} \tag{12}$$

In the experiments of Sullins and McLafferty,[11] the Mach number of the inflow air was 2.0, and the duct was a square measuring 0.8 inch by 0.2 inch. In their experiments, three kinds of wall geometry were adopted: no step, a 0.05-inch backward-facing step, and a 0.1-inch step. When the steps were located upstream of the pseudo-shock, the base pressure at the step was estimated with an empirical equation.[16] In the present model, two pressures, that is, the pressure at the starting position and the pressure at the end of the pseudo-shock, are specified. Therefore, when the step was in the pseudo-shock, as shown in Fig. 4., the base pressure, P_{step}, was calculated using linear interpolation, as below:

$$P_{step} = \frac{P_p - P_1}{L_p} \cdot L_{step} + P_1 \tag{13}$$

In the experiments of Neumann and Lustwerk,[17] the throat and the nozzle exit diameters were specified. The pressure at the exit of the supersonic nozzles was 0.002 and 0.003, being normalized with total pressure. In the experiments of Ostras and Penzin,[4] the Mach
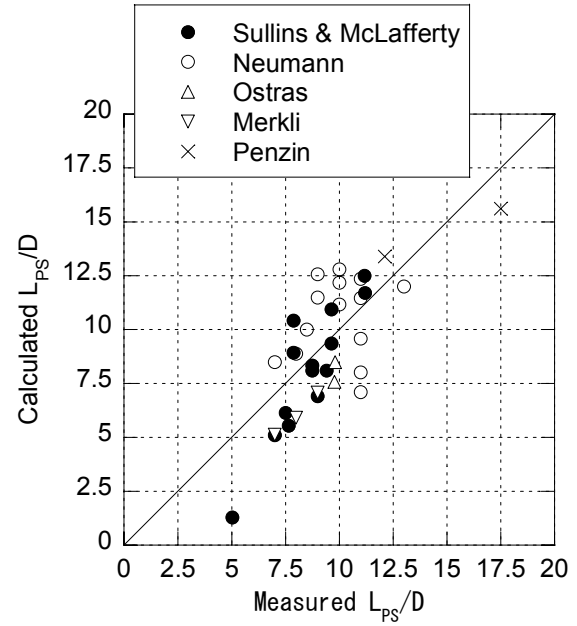

Fig. 3 Comparison of calculated length of pseudo-shock with measured length in straight ducts.

number was 3.1, while that in the experiments of Merkli[18] was 2.8. In the experiments of Penzin,[12] the Mach number was 3.8. In his test, a square duct was set in the inviscid core flow of the wind tunnel. Though there are disagreements of several duct height in length of the pseudo-shock, the prediction accuracy seems to be sufficient within the scope of preliminary application. The correlation coefficient between the calculated values and the measured ones was 0.75.
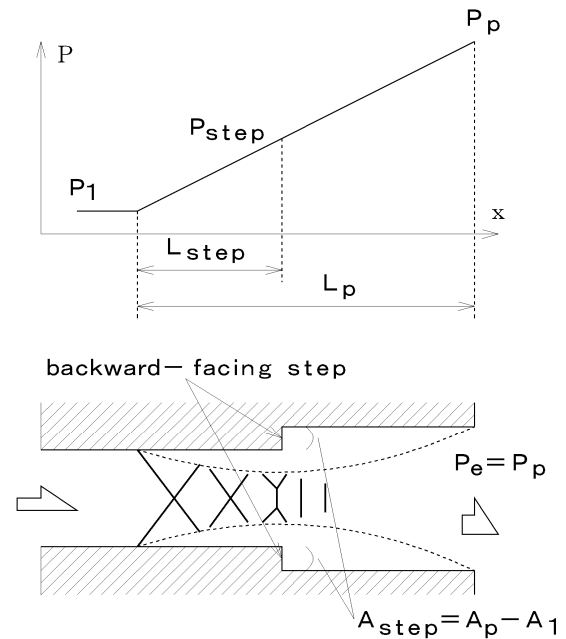

Fig. 4 Pressure at the step in the pseudo-shock. The pressure is interpolated linearly with pressure of the inflow and pressure at the end of pseudo-shock.

The length of the pseudo-shock can be estimated with the diffusion model of Eq. (14) [7] and the empirical equation of Eq. (15) [10,11] as below.

$$\frac{L_p}{D} = \frac{2}{0.114}\sinh^{-1}\left(\frac{w_1 - w_p}{2w^*}\right) \qquad (14)$$

$$\frac{L_p(M_1^2 - 1)\cdot \mathrm{Re}_\theta^{1/4}}{D^{1/2}\cdot \theta^{1/2}} = 50\left(\frac{P_p}{P_1} - 1\right) + 170\left(\frac{P_p}{P_1} - 1\right)^2 \qquad (15)$$

Most of the lengths calculated with the diffusion model of Eq. (14) were larger than the measured ones, and the correlation coefficient was 0.50. Most of the lengths predicted with the empirical equation of Eq. (15) were larger than the measured ones, and the correlation coefficient was 0.23. The lengths calculated with the empirical equation were much smaller than the measured ones of Penzin. This was caused by the thin momentum thickness in his experiments. In the calculation of the lengths with the diffusion model or the empirical equation, the reaction force at the step was not included. This is one of the reasons for the disagreement in the results of the two methods.

The calculated results are affected by the friction coefficient. Here, the formula of van Driest was used. When the formula of White[19] was used, the friction coefficient was smaller by about 10%, and the length of the pseudo-shock was shorter. Therefore, which formula should be adopted is problematic. The formula of White is as below.

$$C_f \approx \frac{0.455}{S^2 \ln\left(\frac{0.06}{S}\cdot \mathrm{Re}_x \frac{\mu_e}{\mu_w}\sqrt{\frac{T_e}{T_w}}\right)} \qquad (16)$$

$$S = \frac{\sqrt{\frac{T_{aw}}{T_e} - 1}}{\sin^{-1} A + \sin^{-1} B} \qquad (17)$$

The Reynolds number also affects the length of the pseudo-shock through the friction coefficient.

Most of the measured lengths were larger than 7 in Fig. 3. The pseudo-shock is composed of oblique and normal shock waves, so a supersonic flow would require some distance to become a subsonic flow.

B. Effect of Backward-Facing Step on Starting Position of Pseudo-Shock

A backward-facing step is used as a flame holding in the scramjet combustor and the dual-mode combustor. The step is also used in the combustor to suppress upstream extension of the pseudo-shock, as well as to hold flame. The starting positions of the pseudo-shock expected to stay at the step for some increase of pressure at the duct exit and this effect of the step on the pseudo-shock has been investigated.[11,20] However, the effectiveness of the step was not proved in the experiments and the reason has not been made clear. The effect of the backward-facing step on the starting position of the pseudo-shock is discussed here from the viewpoint of the momentum balance.

The lengths of the pseudo-shock in the flow with the step predicted by the present model are plotted in Fig. 3 as the results of Sullins and McLafferty.[11] In their experiments, the inflow Mach numbers were 2 or 2.85. The ratios of the step height to the duct height upstream of the step were 0.125 or 0.25. The ratio of the pressure at the end of the pseudo-shock to that of the inflow was up to 4. In the experiments of Matsuura, et al., the inflow Mach number was 2.3 and the ratios of the heights were from 0.05 to 0.4. The ratio of the pressures was up to 5.[20] Figure 4 shows the condition that the starting position of the pseudo-shock locates upstream of the step.

When there is a backward-facing step upstream of the pseudo-shock, pressure at the step, P_{step}, is usually much lower than pressure of the primary flow, P_1.[16] Therefore, the increase of the impulse function, $A_{step}\cdot P_{step}$, is small in comparison with the function of the inflow. On the other hand, the increase of the impulse function due to the area increase of A_{step} at the exit of the duct, that is, the end of the pseudo-shock, $A_{step}\cdot P_p$, is larger than the increase at the step of $A_{step}\cdot P_{step}$ because of the greatly higher pressure at the exit of the pseudo-shock, P_p, than the pressure at the step, P_{step}. The difference in the increase of the impulse function of $A\cdot P$ between the step and the exit, $(A_{step}\cdot P_p - A_{step}\cdot P_{step})$, should be in the same order of the magnitude of the friction upstream of the pseudo-shock to match the inflow and outflow impulse functions.

The above discussion is expressed in equations as

follows. The flow is subsonic at the exit of the pseudo-shock, and the Mach number, M_p, is lower than unity. A ratio of the momentum to the pressure force is lower than unity.

$$\left(\dot{m} \cdot u\right)_p \big/ \left(A \cdot P\right)_p = \left(\gamma \cdot M^2\right)_p$$
$$< 1 \tag{18}$$

The impulse function of the duct with no step is expressed as follows.

$$F_1 = \left(\dot{m} \cdot u_{nostep} + A_1 \cdot P\right)_p + f_{f,nostep}$$
$$\approx A_1 \cdot P_p + f_{f,nostep} \tag{19}$$

The impulse function of the duct with the step is expressed as follows.

$$F_1 = \left[\dot{m} \cdot u_{step} + \left(A_1 + A_{step}\right) \cdot P\right]_p - A_{step} \cdot P_{step} + f_{f,step}$$
$$= \left(\dot{m} \cdot u_{step} + A_1 \cdot P\right)_p + A_{step} \cdot P_p - A_{step} \cdot P_{step} + f_{f,step}$$
$$\approx A_1 \cdot P_p + A_{step} \cdot \left(P_p - P_{step}\right) + f_{f,step} \tag{20}$$

By equating the right-hand terms of Eqs. (19) and (20), the frictions of the duct with no step and the duct with the step are related as follows.

$$f_{f,nostep} \approx f_{f,step} + A_{step} \cdot \left(P_p - P_{step}\right)$$
$$> f_{f,step} \tag{21}$$

Here,

$$P_{step} \big/ P_1 < P_{step} \big/ P_p$$
$$<< 1 \tag{22}$$

Therefore, in order to reduce friction, the starting position of the pseudo-shock shifts further upstream than the position in the flow with no step. The backward-facing step is not effective to suppress upstream extension of the pseudo-shock.

When there is step, the starting position of the pseudo-shock reaches the step position with a smaller increase of the exit pressure than the increase in a duct with no step. Once the starting position of the pseudo-shock is at the step, the starting position stays at the step and the pressure at the step increases with the increase of the exit pressure in order to match the impulse function at the step position with the outflow impulse function.

When the backward-facing step is in the pseudo-shock or downstream of the shock, the pressure at the step, P_{step}, is close to that at the exit of the pseudo-shock, P_p. The increase of the impulse function downstream of the step, $A_{step} \cdot P_{step}$, is also close to the increase at the exit of the pseudo-shock, $A_{step} \cdot P_p$. Therefore, the starting position of the pseudo-shock is located almost at the same position as in the flow with no step. When the backward-facing step is in the pseudo-shock or downstream of the shock, the backward-facing step does not affect the starting position of the pseudo-shock significantly.

The above discussion is expressed in equations as follows. When the step is in the pseudo-shock, a ratio of pressure at the step to that at exit of the pseudo-shock is almost unity, differing from the ratio of Eq. (22) in which the step is located upstream of the pseudo-shock.

$$P_{step} \big/ P_p \approx 1 \tag{23}$$

Then, the frictions are related as follows, differing from the relation expressed in Eq. (21).

$$f_{f,nostep} \approx f_{f,step} + A_{step} \cdot \left(P_p - P_{step}\right)$$
$$\approx f_{f,step} \tag{24}$$

Therefore, the starting position of the pseudo-shock is located almost at the same position as in the flow with no step.

The experimental results[11,20] showed the features discussed here although the suppression of the upstream extension of the pseudo-shock was expected by the step.

C. Pseudo-Shock in a Divergent Duct

Figure 5 shows a comparison of the lengths of a pseudo-shock calculated with the present model and the ones measured in the divergent duct. Here, the end position of the pseudo-shock was at the end of the pressure increase in the duct. The length of the pseudo-shock, L_p, is normalized with the length of the divergent duct, L_{div}. In the divergent duct, the diameter at the entrance is different from that at the exit, and the mean diameter for the pseudo-shock depends on its starting position. So, the length of the divergent duct is used for normalization, though the hydraulic diameter is used in the straight duct. When the length is larger than the length of the divergent duct, the starting position of the pseudo-shock is in the straight duct upstream of the divergent duct. The inflow air expands isentropically from the entrance to the pseudo-shock.

In the present model, two pressures, that is, the pressure at the starting position and the pressure at the end of the pseudo-shock, are attained or specified. Therefore, linear wall pressure distribution is presumed in the pseudo-shock, and reaction force in the pseudo-shock is calculated with this pressure. In the experiments of Penzin,[12] three Mach numbers were adopted. In his test, a square duct was set in the inviscid core flow of the wind tunnel. The divergent angle was 0.5, 1.0, 2.0, or 3.0 degrees. In the experiments of Ikui and others,[13] the inflow Mach number was 1.8, and the divergent half angle was 2.2 or 4.2 degrees. When the starting position of the pseudo-shock was around the entrance of the divergent duct, the lengths calculated with the present model were larger than measured ones. However, the calculated values showed smaller disagreement with the measured ones when the starting position of the pseudo-shock was within the divergent duct, that is, $L_p/L_{div} < 1$. This simple model will be useful for, e.g., preliminary design of a diffuser, when $L_p/L_{div} < 1$. The correlation coefficient was 0.75.

Figure 6 shows the ratio of calculated friction force to calculated reaction force, $f_{f1}/(f_{r1}+f_{rp})$, in the divergent duct when the calculated length of the pseudo-shock was shorter than the length of the divergent duct. Since the present model presumes no friction in the pseudo-shock, the friction force became smaller than the reaction force with the increase of the length of the pseudo-shock. Since the estimated lengths of the pseudo-shock approximately agreed with the measured ones, the estimated ratios of the forces probably agree with the actual ratios. As the pseudo-shock becomes longer, the reaction force in the pseudo-shock is significantly larger than the friction force. When the pseudo-shock covers most of the divergent duct, the length of the pseudo-shock is primarily specified with the reaction force from the wall in the pseudo-shock. Therefore, choice of formula on the friction coefficient or the Reynolds number within the turbulent boundary layer is not a dominant problem in the divergent duct, nor is choice of method to calculate the reaction force upstream of the pseudo-shock, for example, the one-dimensional flow model, the Prandtl-Meyer function, or the method of characteristics.

The accuracy of the length of the pseudo-shock is not affected in the straight duct by the pressure distribution, whereas it is affected in a divergent duct. The accuracy can be improved by modeling of the pressure distribution of the pseudo-shock in a divergent duct, and further study of the flow structure in the pseudo-shock is necessary.

In the present study, the end of the pseudo-shock was presumed at the end of the pressure increase, since it is difficult to specify the end position of the pseudo-shock in the divergent duct, as mentioned at the beginning of Chapter II. When the separation and the pseudo-shock are over upstream of the end of the divergent duct, the attached subsonic gas still flows in the divergent duct with the increase of pressure. Equation (25) shows a relation between an area ratio
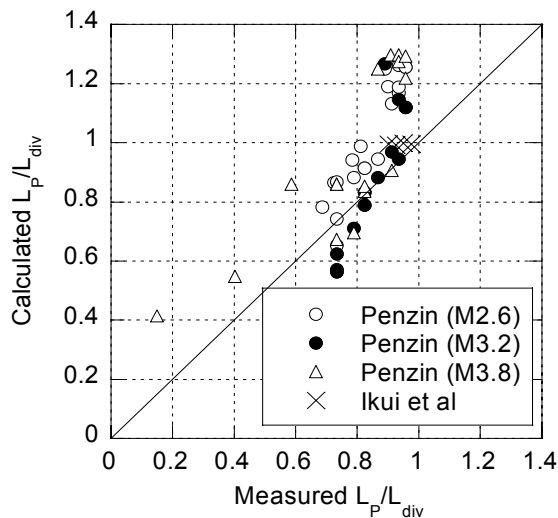

Fig. 5 Comparison of calculated length of pseudo-shock with measured length in divergent ducts.
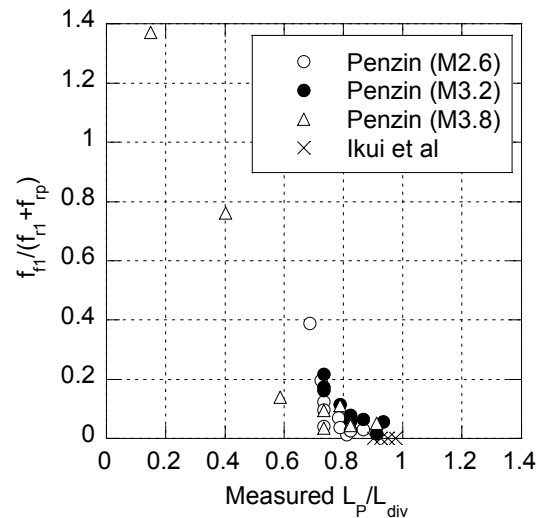

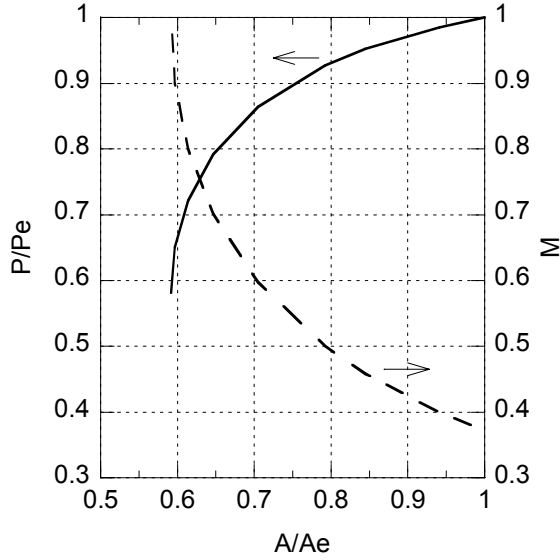Fig. 6 Ratio of friction force to reaction force in the divergent duct.

Fig. 7 Pressure and Mach number changes of the subsonic flow in the divergent duct.

and a ratio of pressure of a subsonic flow to its total pressure in an isentropic change, and Figure 7 shows the pressure ratio of the subsonic flow in a divergent duct. A Mach number of the flow is also plotted.

$$\frac{A}{A_e} = \left(\frac{P_e}{P}\right)^{\frac{\gamma+1}{2\gamma}} \sqrt{\frac{\left(\frac{P_t}{P_e}\right)^{\frac{\gamma-1}{\gamma}} - 1}{\left(\frac{P_t}{P}\right)^{\frac{\gamma-1}{\gamma}} - 1}} \qquad (25)$$

In this sample calculation, the ratio of the total pressure to the static pressure of the flow at the exit is 1.1. At this condition, the Mach number is 0.37 at the exit. The pressure gradually increases with an increase of the area ratio. At that time, friction also works in the divergent duct downstream of the pseudo-shock, that is, in the attached flow area, even under the condition of the pressure increase, and the total friction force is larger than the value presumed in the present model calculation. This flow condition will affect the accuracy of the model calculation. This should be included in the study of the modeling of the pressure distribution of the pseudo-shock in a divergent duct.

D. Flow Field Downstream of Pseudo-Shock

When a long straight duct is used for tests, the end of the pseudo-shock, namely, the point with the highest pressure, may appear in the middle of the duct

and pressure decreases to the value at the downstream boundary. Downstream of the shock, the boundary layer would become reattached to the duct wall, and the friction force would again come into play. Figure 8 shows calculated results of the shear stress downstream of the pseudo-shock in comparison with the shear stress at the end of the supersonic facility nozzle. The friction coefficient downstream of the shock was calculated with a curve-fit equation.[21] The flow conditions were based on the experimental results of Neumann and Lustwerk[17] and Merkli.[18] The stress was the average of the stress at the end of the pseudo-shock and the stress at the exit of the duct.

The shear stress in the downstream subsonic region was about half of that in the upstream supersonic region. When L_{f2} is not short, the effect of friction downstream of the pseudo-shock, f_{f2}, must be included in the force balance. The friction works in the region with the length of L_{f2}. Though another condition is required to specify the length of L_{f2}, it has not been found yet. In the present study, this momentum balance model is applied only to a flow field in which L_{f2} is short.

E. Dual-Mode Combustor

This model was applied to dual-mode combustion tests.[22] In the dual-mode engine, an isolator is installed between the inlet and the combustor to isolate high pressure in the combustor from the inlet. Supersonic airflow from the inlet is decelerated to subsonic velocity through the pseudo-shock in the isolator in
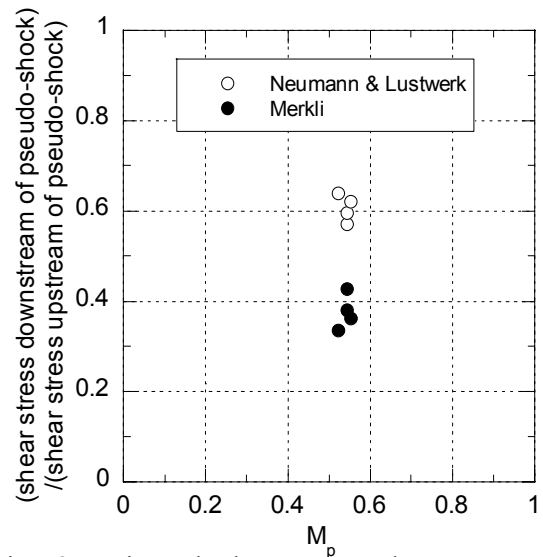

Fig. 8 Estimated shear stress downstream of pseudo-shock in a straight duct, normalized with the shear stress upstream of the shock.

the ramjet mode.[23] Generally, the isolator is a straight duct and optimization of its length is required in the design of the engine. Figure 9 shows a schematic diagram of the experimental facility. Mach 2.5 air heated by a vitiation heater flowed into the duct. Total temperature and total pressure were 800 K and 1.0 MPa, respectively. Hydrogen fuel was injected into the subsonic airflow at sonic speed perpendicular to the wall from injector 1 or injector 6. Due to the location of the fuel injection, two kinds of the ramjet mode were attained, namely, the normal ramjet mode and the downstream-combustion ramjet mode.[24] In the normal ramjet mode, airflow was decelerated in the isolator through the pseudo-shock, and fuel was injected from injector 1. Combustion gas choked thermally at the exit of the upstream straight duct. In the downstream-combustion ramjet mode, airflow was decelerated in the divergent duct and fuel was injected from injector 6. Combustion gas choked thermally at the exit of the downstream straight duct.

In the calculation, combustion gas was in the equilibrium condition. The friction coefficient in the upstream supersonic region of L_{f1} was calculated with the formula of White.[19] In the region of the pseudo-shock, no fuel was presumed. In the experiments, it was found that the injected fuel did not flow upstream significantly in the pseudo-shock.[22] The highest pressure at the end of the pseudo-shock was the downstream boundary condition in the normal ramjet mode. The highest pressure was specified with combustion efficiency. Combustion gas choked thermally at the exit of the upstream straight duct under the presumed efficiency. In the downstream-combustion ramjet mode, the downstream boundary condition was characterized by choking at the exit. The portion of the duct between the fuel injector and the exit of the duct was short, so friction downstream of the pseudo-shock, f_{f2}, namely, friction in the L_{f2} region, was omitted in the calculation.

Figure 10 shows distributions of the measured and the calculated pressures in the normal ramjet mode. The origin of the x axis is at the step. In the experiment, maximum pressure was attained in the vicinity of the fuel injector. The starting position of combustion was set at the fuel injector location in the calculation. Combustion efficiency was estimated to be 0.75 based on the measured peak pressure. Combustion gas choked thermally at the end of the straight duct, indicated as 'throat' in the figure. The calculated pressures at the starting position and at the end of the pseudo-shock were connected linearly, because only two pressure values were attained or specified. The starting position of the pseudo-shock predicted by the present model reasonably agreed with that in the test.
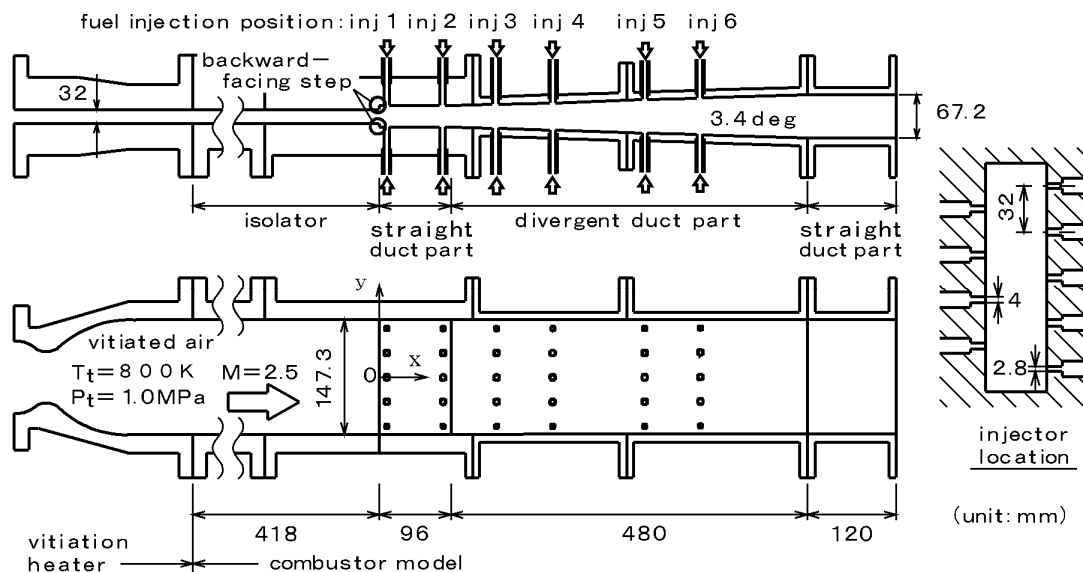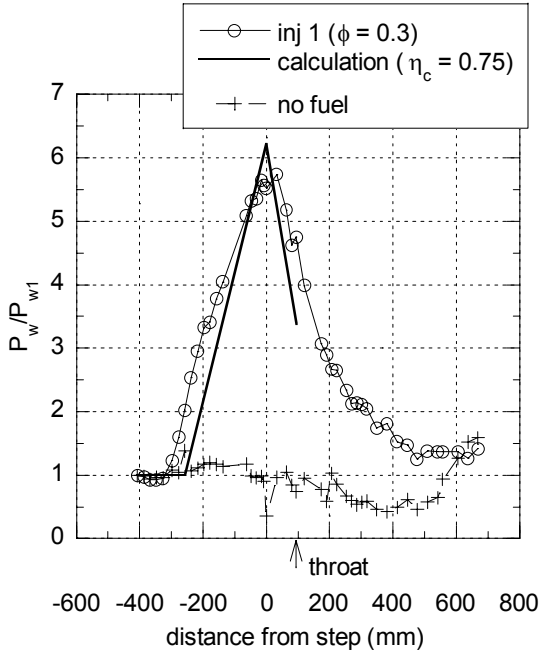

Fig. 9 Schematic of dual-mode combustor.

Fig. 10 Pseudo-shock length in the normal ramjet mode. Fuel was injected at inj 1 of Fig. 8.
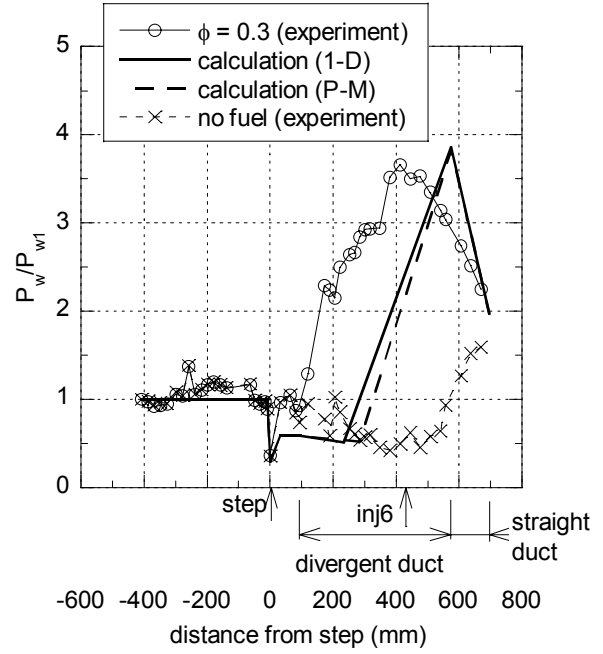

Fig. 11 Pseudo-shock length in the downstream combustion ramjet mode. Fuel was injected at inj 6 in the experiment and at junction of the ducts in the calculation. Combustion gas choked thermally at the exit.

From the balance of the momentum, the following feature of the dual-mode combustor is clarified. The impulse function at the choking condition is expressed as follows with Eq.(2).

$$F_e = \dot{m} \frac{\sqrt{\gamma \cdot R \cdot T_t}}{\sqrt{1 + \frac{\gamma - 1}{2}}} \left(1 + \frac{1}{\gamma}\right) \qquad (26)$$

When the impulse function at the exit of the combustor under the choking condition is larger than the impulse function of the inflow air, the engine cannot keep the pseudo-shock in an isolator of any length. The largest thrust is attained when the function under the choking condition is the same as that of the inflow air to the isolator. Thus, under this condition, the starting position of the pseudo-shock is at the entrance of the isolator.

Figure 11 shows distributions of the measured and the calculated wall pressures in the downstream-combustion ramjet mode. In the experiment, fuel was injected from injector 6. In the present calculation, the chemically equilibrium condition was presumed to calculate gas properties and distribution of combustion efficiency was not presumed. Therefore, the combustion position was set at the junction of the divergent duct and the downstream straight duct, located downstream of injector 6. Combustion

efficiency was set to be 0.90 based on the measured combustion efficiency.[22] From this efficiency, total temperature of the combustion gas was calculated with the experimentally measured mass flow rates of the gases. With the choking condition, the impulse function of the outflow combustion gas was calculated with Eq. (26). The impulse function of the subsonic mixture was equal to the impulse function of the combustion gas at the junction of the ducts. This impulse function and the pressure of the mixture were calculated with Eqs. (1) and (2). This pressure of the mixture is the maximum pressure at the exit of the pseudo-shock. The calculated pressures at the starting position and at the end of the pseudo-shock were connected linearly, because the two pressures were attained or specified with the present model. Two methods for estimating the reaction force in the divergent duct upstream of the pseudo-shock were examined. In one, pressure was calculated one-dimensionally and isentropically. The result is indicated as 1-D in the figure. In another, pressure was calculated with the two-dimensional Prandtl-Meyer function. The result is indicated as P-M. f_{rp} was calculated with the pressure at the starting position of the pseudo-shock and the pressure at the end, presuming a linear distribution of wall pressure.

Downstream of the step, the pressure, being calculated with the empirical equation,[16] decreased due to expansion.

In the experiment, combustion commenced at the injector position of $x = 433$ mm and the pressure began to decrease, though the cross section further increased until the end of the divergent section. The heat release position moved downstream in the calculation, and the starting position of the pseudo-shock also shifted downstream approximately the same distance. The calculated pressure at the end of the pseudo-shock reasonably agreed with the measured highest pressure, as well as the length of the pseudo-shock. In this simulation, the downstream boundary condition was characterized by choking at the exit. With the present model, it was possible to predict the pseudo-shock pressure.

The starting position of the pseudo-shock calculated with the one-dimensional model was close to that calculated with the Prandtl-Meyer function. There was no large difference in reaction forces between the two results because the reaction force was primarily affected by higher pressure and larger area of the pseudo-shock.

F. Diffuser of Ejector

In the ejector, the primary supersonic flow and the secondary subsonic flow are mixed and decelerated through the pseudo-shock. The present model was applied to this two-flow condition. In aerodynamic experiments of the ejector-jet, a choking condition was applied at the exit of the duct by throttling, which simulated subsonic combustion and subsequent choking.[25] Figure 12 shows a schematic of the test model. The primary flow was Mach 2.4 air and the secondary flow was subsonic nitrogen. In the calculation, the primary flow and the secondary flow were assumed to interact downstream of the nozzles and flow in parallel under the same pressure with no mixing. Friction was calculated under this condition after the interaction upstream of the pseudo-shock. The friction coefficient was calculated with the formula of van Driest.[15] The flows mixed through the pseudo-shock, decelerated and choked at the throat by throttling. The impulse function at the end of the pseudo-shock upstream of the throat was calculated in the isentropic process with the properties at the throat under the choking condition. f_{f1} was determined to keep balance of the inflow and outflow impulse functions.

Figure 13 shows experimental and calculated distributions of pressure. The subsonic secondary flow choked aerodynamically in the test section downstream of the nozzle exit. The ratio of the total pressure of the secondary flow to that of the primary flow, P_{t2}/P_{t1}, was 0.04. The ratio of the area of the secondary flow to that of the primary flow, A_2/A_1, was 0.81. The ratio of the downstream throat height to that of the primary flow, H_{th}/H_1, was 1.56 under the throttling condition. In the experiments, pressure was measured on the primary-flow sidewall. Figure 14 shows the results when $A_2/A_1 = 0.57$. P_{t2}/P_{t1} and H_{th}/H_1 were the same as those of Fig.13. The calculated pressures at the staring position and at the end of the pseudo-shock were connected linearly, because the two pressures were attained or specified in the present model.
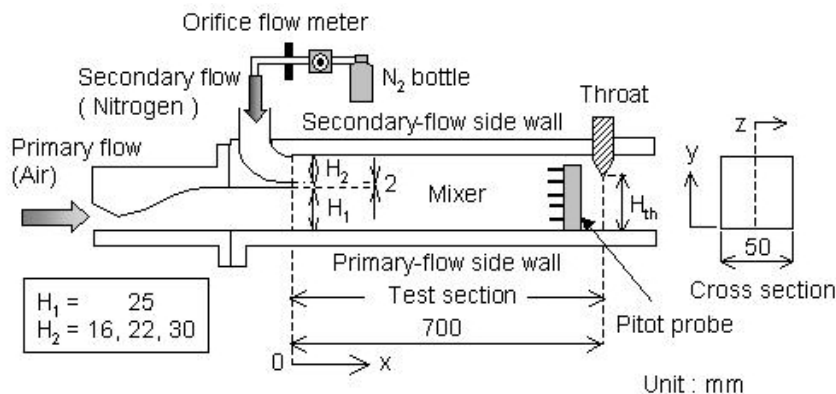

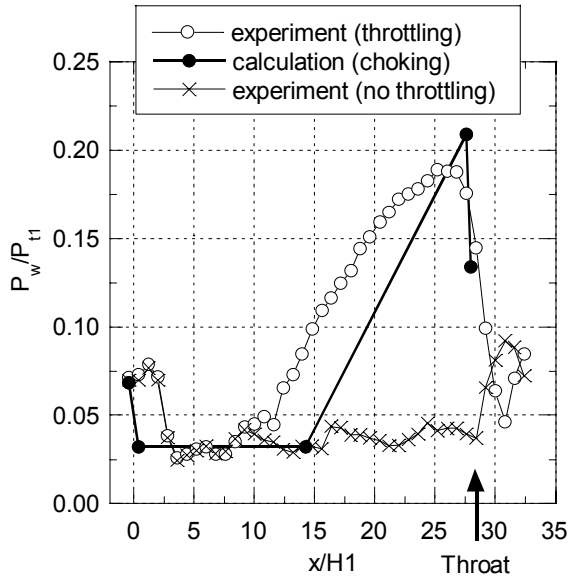Fig. 12 Schematic of aerodynamic test model of ejector-jet.

Fig. 13 Calculated and measured pressure distributions in the ejector-jet model. Ratio of area of the secondary flow to that of the primary flow was 0.81.
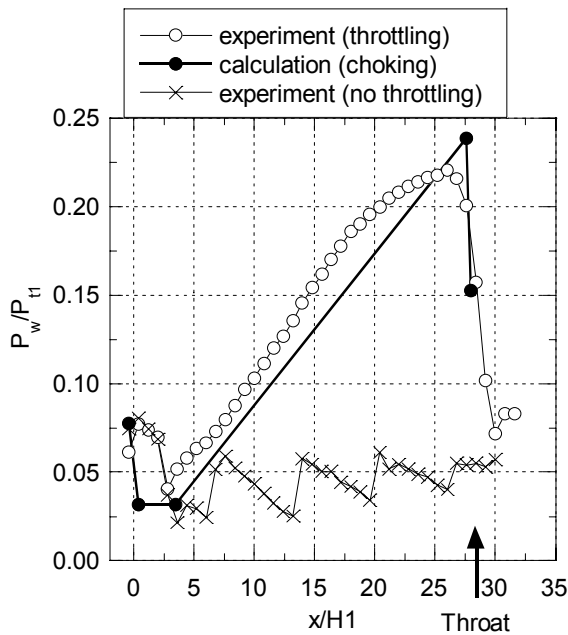

Fig. 14 Calculated and measured pressure distributions in the ejector-jet model. Ratio of area of the secondary flow to that of the primary flow was 0.57.

The lengths of the pseudo-shock reasonably agreed with those of the experiment. Here, specified pressure was not applied to the downstream boundary, but the choking condition was applied. The pressures at the end of the pseudo-shock also reasonably agreed with the measured pressures. The pressure at the end of the pseudo-shock corresponds to the pressure behind the normal shock of the mixed flow including the effect of

the boundary layer.[14] This model will be useful for preliminary design of a diffuser of the ejector system.

G. Starting Position of the Pseudo-Shock
(a) Effect of thickness of boundary layer

It is well known that the pseudo-shock becomes longer as the inflow boundary layer becomes thicker. Waltrup and Billig constructed their empirical equation of Eq. (15) in which length of the pseudo-shock increases with an increase in the momentum thickness of the inflow boundary layer.[6] This feature is discussed with the momentum balance model in a straight duct as shown in Fig. 1.

As the inflow boundary layer becomes thicker, the mass flow rate and the impulse function of the inflow become smaller. When pressure is specified at the exit, the outflow impulse function is also specified with conservation of the mass flow rate. Figures 15 (a) and (b) show sample calculation results. The normalized impulse function at the exit of the straight duct, F_e/F_i, is plotted in relation to the normalized height of the inflow boundary layer. F_i included the effect of the inflow boundary layer. Mach numbers of the inflow air in the inviscid core flow were 4 and 2. The ratios of pressure specified at the exit, P_e, to that at the entrance, P_i, were 14 at Mach 4, and 3.8 at Mach 2. The 1/7 power-law velocity distribution was presumed in the boundary layer. As the height of the inflow boundary layer increased, the outflow impulse function approached the inflow impulse function, that is, the difference between the inflow and outflow impulse functions decreased. A smaller decrease of inflow impulse function due to friction was required upstream of the pseudo-shock. In Fig. 15 (b), L_{f1} is indicated, being normalized with a hydraulic diameter. The friction coefficient was set to be 0.001. The starting position of the pseudo-shock shifted upstream as the inflow boundary layer thickened. In the present calculations, the normalized heights of the boundary layer smaller than about 0.5 were necessary to locate the pseudo-shock within the duct.
(b) Effect of pressure or throttling at downstream boundary

When the pressure at the exit is the downstream boundary condition and is increased, the Mach number at the exit decreases and the outflow impulse function increases (Eqs. (1) and (2)). Then, the starting position
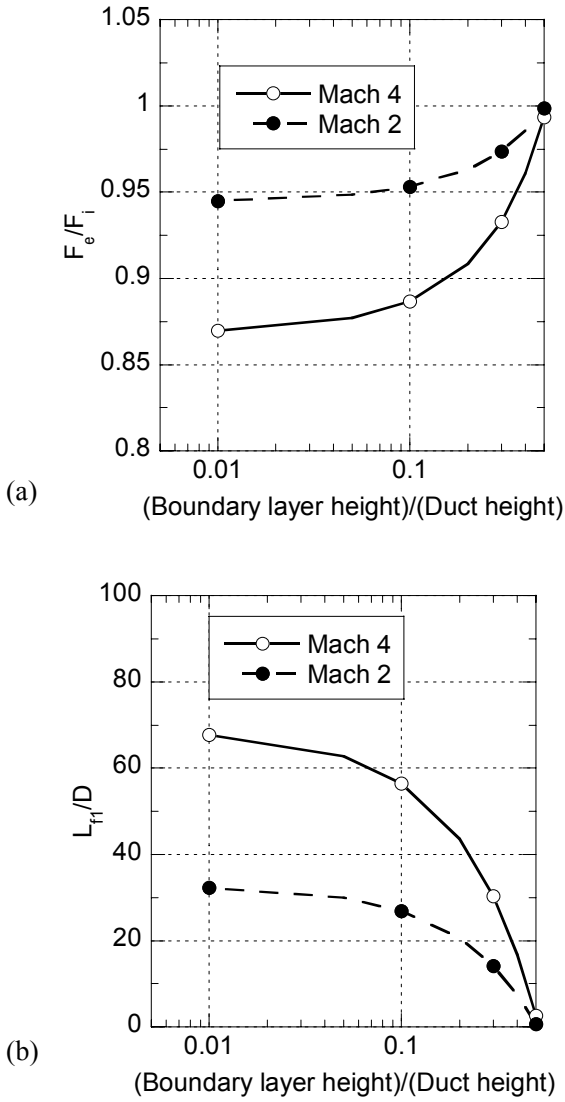
(a)

(b)

Fig. 15 Effect of boundary layer on starting position of pseudo-shock. (a) Normalized impulse function at the exit of the straight duct. (b) Normalized length upstream of the pseudo-shock.

of the pseudo-shock shifts upstream.

When choking is applied by throttling as the downstream boundary condition, the outflow impulse function does not change due to the area change at the throat itself, as can be seen in Eq. (2). Throttling

increases the ratio of the upstream subsonic sectional area to the throat sectional area and decreases the Mach number upstream of the throat. The throttling increases the impulse function of the subsonic flow upstream of the throat as seen in Eq. (2) with the decrease of the Mach number. Therefore, throttling shifts the starting position of the pseudo-shock upstream.

(c) Effect of bleeding

Bleeding is used to suppress the upstream extension of the pseudo-shock by decreasing thickness of the boundary layer.[1,26] This effectiveness is explained from the viewpoint of momentum balance here. Figure 16 is a schematic of bleeding in a straight duct. Subscript 1b indicates gas flow after bleeding and upstream of the pseudo-shock. Here, pressure is assigned at the exit of the duct. Mass and force are independent conservation items, respectively. When part of mass is bled perpendicular to the flow direction as shown in Fig. 16, then the mass flow rate decreases, but the impulse function does not decrease by bleeding.

$$\dot{m}_{1b} = \dot{m}_1 - \dot{m}_b \tag{27}$$

$$F_{1b} = F_1 - f_{f1} \tag{28}$$

$$F_2 = F_{1b} \tag{29}$$

Here, the starting position of the pseudo-shock is presumed to be at the downstream edge of the bleeding region. F_1 is the impulse function upstream of the bleeding and F_{1b} is the impulse function at the downstream of the bleeding, namely, at the starting position of the pseudo-shock. Eq. (29) stands up irrespective of the flow structure in the pseudo-shock when friction on the wall is sufficiently small in the pseudo-shock.

Figures 17 (a) and (b) show sample calculation results. The normalized impulse function at the exit of the duct, F_2/F_{1b}, is plotted in relation to the bleeding
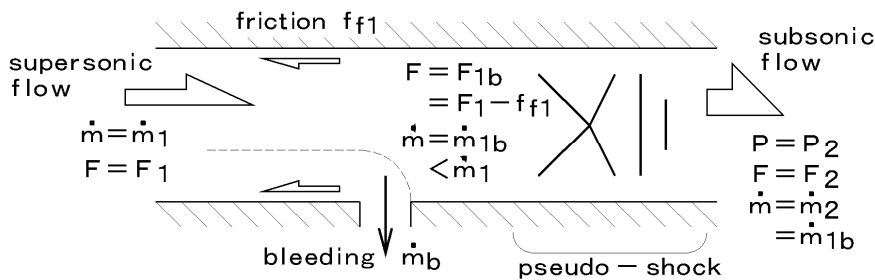

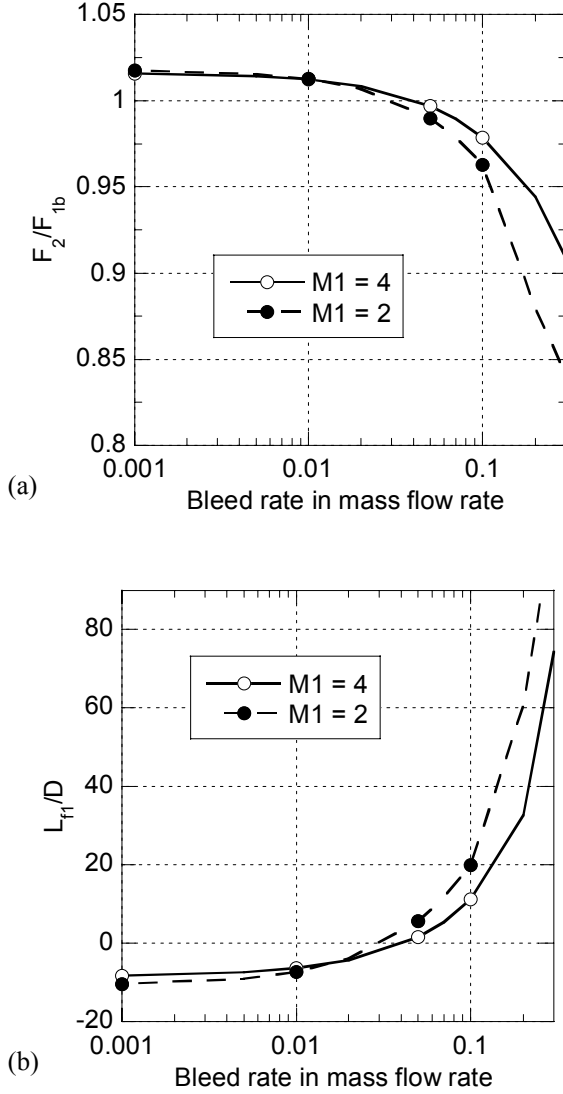Fig. 16 Schematic of bleeding in a straight duct.

(a)

(b)

Fig. 17 (a) Impulse function at the exit and (b) length upstream of pseudo-shock in relation to bleeding rate. The ratio of pressure at the exit to that at the entrance was 19 at Mach 4, whereas it was 4.7 at Mach 2.

rate, $\dot{m}_b / \dot{m}_1$. Mach numbers of the inflow air are 4 and 2. The ratios of pressure specified at the exit, P_2, to that at the entrance, P_1, were 19 at Mach 4, and 4.7 at Mach 2. These ratios are larger than the ratios across the normal shock, and usually the pseudo-shock cannot stay in the duct with no bleeding.

Due to the decrease of the mass flow rate, the impulse function at the exit decreases when pressure is specified at the exit. That is, the Mach number decreases by bleeding under the assigned pressure condition at the exit, as seen in Eq. (1). The impulse function is expressed as

$$F = A \cdot P \left(1 + \gamma M^2 \right) \tag{30}$$

As can be seen in Eq. (30), a decrease of Mach number induces a decrease of impulse function under the specified pressure condition. The normalized impulse function decreased to unity as the bleeding rate increased. In Fig. 17 (b), the length upstream of the pseudo-shock, L_{f1}, is indicated, being normalized with a hydraulic diameter. The friction coefficient was set to be 0.001. Negative L_{f1} expresses the condition that the pseudo-shock cannot stay in the duct. In the present calculations, bleeding rates larger than about 0.03 were necessary to locate the pseudo-shock within the duct. Further decrease of the impulse function at the exit permits further decrease of the inflow impulse function by friction in the duct. Bleeding is effective for suppression of upstream extension of a pseudo-shock, but the effectiveness is caused by a decrease of the impulse function at the exit of the duct.

IV. Conclusion

The momentum balance model of a flow field with a pseudo-shock was presented. In this simple model, no friction is presumed in the region of the pseudo-shock. The outflow impulse function is balanced with the inflow impulse function, friction, and reaction force by adjusting the starting position of the pseudo-shock. The length of the pseudo-shock was determined from the adjusted starting position of the pseudo-shock. This model cannot be applied to a flow with a Mach number below 1.5 nor to a flow in a long duct. The calculated lengths of the pseudo-shock were compared with the experimental ones in the straight ducts and the divergent ducts. Test results of the ejector were also compared with the results calculated with the present model. One of the two downstream boundary conditions, namely, specified pressure boundary or choking, was applied. The pseudo-shock pressure was also compared under the choking condition.

Calculated results showed reasonable agreement with the experimental results in length and pressure within the scope of preliminary application. In the present study, the end of the pseudo-shock was presumed at the end of the pressure increase. This affects the accuracy of the predicted length of the pseudo-shock as well as the linear interpolation of the pressure distribution in the pseudo-shock, especially in the divergent duct.

Several features of the pseudo-shock were also discussed with the present model or from the viewpoint of the momentum balance and the following points were clarified. The backward-facing step is not effective for suppression of upstream extension of the pseudo-shock. The starting position of the pseudo-shock is primarily dominated by the reaction force in a divergent duct. The required length of the isolator of the dual-mode engine depends on the balance of the inflow impulse function of air and the outflow function of the combustion gas under choking. Effects of height of the boundary layer, pressure at the exit of the duct, throttling and bleeding on the starting position of the pseudo-shock were also explained from the viewpoint of momentum balance.

References

[1]Matsuo, K., Miyazato, Y., and Kim, H.-D., "Shock Train and Pseudo-Shock Phenomena in Internal Gas Fows," *Progress in Aerospace Sciences*, No. 35, 1999, pp. 33-100.

[2]Crocco, L., "One-Dimensional Treatment of Steady Gas Dynamics," Fundamentals of Gas Dynamics, Vol. 3, High Speed Aerodynamics and Jet Propulsion, 1958, Princeton University Press, Princeton, NJ, pp. 100-130.

[3]Waltrup, P. J., and Cameron, J. M., "Wall Shear and Boundary-Layer Measurement in Shock Separated Flow," *AIAA Journal*, Vol. 12, No. 6, 1974, pp. 878-880.

[4]Ostras, V. N., and Penzin, V. I., "Experimental Study of Friction in a Channel with a Pseudoshock," *Fluid Mechanics – Soviet Research*, Vol. 4, No. 6, 1975, pp. 32 – 38.

[5]Carroll, B. F., and Dutton, J. C., "Characteristics of Multiple Shock Wave/Turbulent Boundary-Layer Interactions in Rectangular Ducts," *Journal of Propulsion and Power*, Vol. 6, No. 2, 1990, pp. 186-193.

[6]Heiser, W. H., Pratt, D. T., Daley, D. H., and Mehta, U. B., "Hypersonic Airbreathing Propulsion," AIAA Education Series, AIAA Washington, DC, 1994, pp. 251-256.

[7]Ikui, T., Matsuo, K., and Nagai, M., "The Mechanism of Pseudo-Shock Waves," *Bulletin of the Japan Society of Mechanical Engineering*, Vol. 17, No. 108, 1974, pp. 731-739.

[8]Ikui, T., Matsuo, K., and Sasaguchi, K., "Modified Diffusion Model of Pseudo-Shock Waves Considering Upstream Boundary Layers," *Bulletin of the Japan Society of Mechanical Engineering*, Vol. 24, No. 197, 1981, pp. 1920-1927.

[9]Zimont, V. L., and Ostras, V. N., "Calculation of Pseudo-Shocks in a Cylindrical Duct," *Fluid Mechanics Soviet Research*, Vol. 5, No. 2, 1976, pp. 78-87.

[10]Waltrup, P. J., and Billig, F. S., "Structure of Shock Waves in Cylindrical Ducts," *AIAA Journal*, Vol. 11, No. 10, 1973, pp. 1404-1408.

[11]Sullins, G., McLafferty, G., "Experimental Results of Shock Trains in Rectangular Ducts," AIAA Paper 92-5103, Dec. 1992.

[12]Penzin, V. I., "Deceleration of Supersonic Flows in Smoothly Diverging-Area Rectangular Ducts," *Scramjet Propulsion*, edited by E.T. Curran and S. N. B. Murthy, Vol. 189, Progress in Astronautics and Aeronautics, AIAA, Reston, VA, 2000, pp. 321-337.

[13]Ikui, T., Matsuo, K., Mochiduki, H., Somekawa, K., "Characteristics of Pseudo-Shock in a Divergent Duct," *Journal of the Japan Society of Mechanical Engineering*, Vol. 45, No. 393, 1979, pp. 611-617 (in Japanese).

[14]McLafferty, G., "Theoretical Pressure Recovery Through a Normal Shock in a Duct with Initial Boundary Layer," *Journal of the Aeronautical Sciences*, March 1953, pp. 169-174.

[15]White, F. M., "Viscous Fluid Flow," McGraw-Hill, New York, 1974, pp. 632-640.

[16]Lamb, J. P., and Oberkampf, W. L., "Review and Development of Base Pressure and Base Heating Correlations in Supersonic Flow," *Journal of Spacecraft and Rockets*, Vol. 32, No. 1, 1995, pp. 8-23.

[17]Neumann, E. P., and Lustwerk, F., "Supersonic Diffusers for Wind Tunnels," *Journal of Applied Mechanics*, Vol. 16, No. 2, 1949, pp. 195-202.

[18]Merkli, P. E., "Pressure Recovery in Rectamgular Constant Area Supersonic Diffusers," *AIAA Journal*, Vol. 14, No. 2, 1976, pp. 168-172.

[19]White, F. M., "Viscous Fluid Flow," McGraw-Hill, New York, 1974, pp. 641-646.

[20]Matsuura, K., Futonagane, Y., Takigami, A., Masuya, G., Tani, K., Kudou, K., and Murakami, A., "An Experiment on Scramjet Isolators with Backward-Facing Step," 21st International Symposium on Space

Technology and Science Paper, ISTS 98-a-1-22, Omiya, Japan, May 1998.

[21]White, F. M., "Viscous Fluid Flow," McGraw-Hill, New York, 1974, pp. 485.

[22]Kato, K., Kanda, T., Kobayashi, K., Kudo., K., and Murakami, A., "Downstream Ramjet-Mode Combustion in a Dual-Mode Scramjet Engine," *Journal of Propulsion and Power,* Vol.22, No.3, 2006, pp. 511-517.

[23]Heiser, W. H., Pratt, D. T., Daley, D. H., and Mehta, U. B., "Hypersonic Airbreathing Propulsion," AIAA Education Series, AIAA Washington, DC, 1994, pp. 334-338.

[24]Kanda, T., Chinzei, N., Kudo, K., and Murakami, A., "Dual-Mode Operations in a Scramjet Combustor," *Journal of Propulsion and Power*, Vol. 20, No. 4, 2004, pp. 760-763.

[25]Aoki, S., Lee, J., Masuya, G., Kanda, T., Kudo, K., and Murakami, A., "Experimental Investigation of an Ejector-jet," *Journal of Propulsion and Power*, Vol.21, No.3, 2005, pp. 496-503.

[26]Seddon, J., and Goldsmith, E. L., "Intake Aerodynamics," AIAA Education Series, AIAA, Washington, DC, 1985, pp. 189-216.

JAXA Research and Development Report JAXA-RR-06-037E